Quaternary Science Reviews 30 (2011) 3603–3617

Contents lists available at SciVerse ScienceDirect

Quaternary Science Reviews

journal homepage: www.elsevier.com/locate/quascirev

Geological constraints on glacio-isostatic adjustment models of relative sea-level change during deglaciation of Prince Gustav Channel, Antarctic Peninsula

Stephen J. Roberts[a,1], Dominic A. Hodgson[a,*,1], Mieke Sterken[b,1], Pippa L. Whitehouse[c], Elie Verleyen[b], Wim Vyverman[b], Koen Sabbe[b], Andrea Balbo[a], Michael J. Bentley[c], Steven G. Moreton[d]

[a] British Antarctic Survey, Natural Environment Research Council, High Cross, Madingley Road, Cambridge CB3 0ET, UK
[b] Laboratory of Protistology and Aquatic Ecology, Ghent University, B-9000 Gent, Belgium
[c] Department of Geography, University of Durham, South Road, Durham DH1 3LE, UK
[d] Natural Environment Research Council Radiocarbon Facility, Scottish Enterprise Technology Park, East Kilbride, UK

ARTICLE INFO

Article history:
Received 4 January 2011
Received in revised form
5 September 2011
Accepted 13 September 2011
Available online 26 October 2011

Keywords:
Sea-level
Ice sheets
Deglaciation
Holocene
Palaeolimnology
Antarctica
Satellite-gravity measurements
GRACE satellite

ABSTRACT

The recent disintegration of Antarctic Peninsula ice shelves, and the associated accelerated discharge and retreat of continental glaciers, has highlighted the necessity of quantifying the current rate of Antarctic ice mass loss and the regional contributions to future sea-level rise. Observations of present day ice mass change need to be corrected for ongoing glacial isostatic adjustment, a process which must be constrained by geological data. However, there are relatively little geological data on the geometry, volume and melt history of the Antarctic Peninsula Ice Sheet (APIS) after Termination 1, and during the Holocene so the glacial isostatic correction remains poorly constrained. To address this we provide field constraints on the timing and rate of APIS deglaciation, and changes in relative sea-level (RSL) for the north-eastern Antarctic Peninsula based on geomorphological evidence of former marine limits, and radiocarbon-dated marine-freshwater transitions from a series of isolation basins at different altitudes on Beak Island. Relative sea-level fell from a maximum of c. 15 m above present at c. 8000 cal yr BP, at a rate of 3.91 mm yr^{-1} declining to c. 2.11 mm yr^{-1} between c. 6900–2900 cal yr BP, 1.63 mm yr^{-1} between c. 2900–1800 cal yr BP, and finally to 0.29 mm yr^{-1} during the last c. 1800 years. The new Beak Island RSL curve improves the spatial coverage of RSL data in the Antarctic. It is in broad agreement with some glacio-isostatic adjustment models applied to this location, and with work undertaken elsewhere on the Antarctic Peninsula. These geological and RSL constraints from Beak Island imply significant thinning of the north-eastern APIS by the early Holocene. Further, they provide key data for the glacial isostatic correction required by satellite-derived gravity measurements of contemporary ice mass loss, which can be used to better assess the future contribution of the APIS to rising sea-levels.

1. Introduction

Since the Last Glacial Maximum (LGM) global sea levels have risen by 125+/−5 m (Fleming et al., 1998). Deglaciation of the northern hemisphere ice sheets contributed ~100 m (Clark et al., 2002); the Antarctic Ice Sheet and other small ice sheets supplied the remainder. Most models predict the Antarctic Ice Sheet to have contributed c. 20 m to global sea-level rise with estimates ranging from as much as 37 m (Nakada and Lambeck, 1988) to 12 m (Huybrechts, 1992). More recently, an improved three-dimensional thermomechanical model has suggested a contribution of 14–18 m (Huybrechts, 2002) which is in accord with the 9.5–17.5 m obtained by Philippon et al. (2006). The variability in these estimates highlights the problems involved in reconstructing the Last Glacial Maximum eustatic contributions from Antarctica.

This is because, of the global ice sheets, the Antarctic Ice Sheet has least field data to constrain its past volume and its contribution to global sea-level change (Solomon et al., 2007). Similarly, there is little geological evidence to determine whether dynamical ice discharge or surface melting has dominated the ice sheet mass balance, a question that is typically explored through ocean general circulation models (e.g. Holland et al., 2008). A better understanding of how global ice sheets contributed to sea-level change since the LGM is therefore key to predicting how changes in these ice sheets could influence sea-level in a future warming world. This is especially relevant as in the last Eemian interglacial (Marine Isotope Stage 5e, MIS5e), when temperatures in Antarctica were up to 6 °C

* Corresponding author. Tel.: +44 1223 221635; fax: +44 1223 362616.
E-mail address: daho@bas.ac.uk (D.A. Hodgson).
[1] These authors contributed equally to this work.

0277-3791/$ – see front matter © 2011 Elsevier Ltd. All rights reserved.
doi:10.1016/j.quascirev.2011.09.009

higher (Sime et al., 2009), global sea-level peaked at least 6.6 m (95% probability) higher than today (Jansen et al., 2007; Kopp et al., 2009). In the current and projected period of warming, modelling suggests that a likely upper bound to sea-level by 2100 is 1.4 m (Rahmstorf, 2007). However, these projected sea-level increases do not include potentially large contributions due to the dynamic instability of ice sheets during the current century (Solomon et al. 2007). Taking such variables into consideration, Pfeffer et al. (2008) estimate an upper bound of 2 m of sea-level rise by 2100.

Ice mass loss in Antarctica is strongly dominated by changes in the Amundsen Sea sector of West Antarctica, with significant loss also inferred over the Antarctic Peninsula by models such as the ICE-5G (VM2) model of Peltier (2004) due to the large value of the GIA correction applied. Limited ice mass loss is inferred for most of East Antarctica (Rignot et al., 2008). The net rate of ice loss in 2006 was $-196+/-92$ Gt yr^{-1}, with contributions of $-60+/-46$ Gt yr^{-1}, $-132+/-60$ Gt yr^{-1} and $-4+/-61$ Gt yr^{-1} from the Antarctic Peninsula, West Antarctica and East Antarctica, respectively (Rignot et al., 2008). With a current rate of atmospheric temperature increase several times the global mean ($3.7+/-1.6$ °C century^{-1}compared to $0.6+/-0.2$ °C century^{-1} (Houghton et al., 2001)), the Antarctic Peninsula is a key locality to study the effects of temperature on the cryosphere. The warming, together with changes in the configuration of ocean currents, have resulted in the catastrophic disintegration of seven ice shelves (Hodgson et al., 2006) and accelerated the discharge of 87% of continental glaciers (Cook et al., 2005). These responses look set to accelerate given IPCC predictions that future anthropogenic increases in greenhouse gas emissions will lead to a 1.4–5.8 °C rise in global temperatures by 2100 (Solomon et al., 2007). On the Antarctic Peninsula, most of the effects leading to loss of ice are currently confined to the north. Continued warming in this region will lead to a southerly progression of ice shelf disintegrations along both coasts (Vaughan and Doake, 1996; Hodgson et al., 2006), removing the buttressing effect of the ice shelves and causing accelerated discharge of their feeder glaciers. The total volume of ice on the Antarctic Peninsula is 95 200 km^3, equivalent to 242 mm of eustatic sea-level rise, or roughly half of all the glaciers and ice caps outside of Greenland and Antarctica (Pritchard and Vaughan, 2007). Prediction of the timing of ice shelf disintegration is not yet possible. However, increased warming may lead to the Antarctic Peninsula making a significant contribution to global sea-level.

At present there are relatively few geological constraints on the extent and thickness of the Antarctic Peninsula Ice Sheet since Termination 1. Observations of relative sea-level (RSL) change constitute one of the primary datasets for constraining the geometry, volume and melt history of past and present glacial masses, and can be used by modellers to infer, indirectly, the thickness of the overlying ice through time and its contribution to meltwater influx (Lambeck et al., 1998; Peltier, 1998). RSL is the relative vertical displacement between the sea surface and the land over a period of time. It is influenced by changes in ocean volume (eustatic changes in sea-level) and deformation of the geoid and solid Earth (isostatic changes) that are caused by changes in the mass of overlying ice (Agostinetti et al., 2004).

There are two common methods for providing geological constraints on RSL change. First, studying raised marine landforms (e.g. beaches, deltas), and second, studying isolation basins. In the former case, in Antarctica, raised marine features are typically sampled for organic material such as shells, seal skin, penguin remains, or whalebone, which can provide a radiocarbon age estimate or constraining date for the age of the beach. In the case of isolation basins, sediment cores are taken from lakes close to sea-level along the coastal margin. Prior to deglaciation, and depending on their altitude, these lakes may have been former marine inlets or basins. Following deglaciation, as isostatic rebound outpaced eustatic sea-level rise, they became isolated and transformed into freshwater lakes. The sediment in the lakes records this transition, and can be dated to determine when the basin sill was at sea-level. By applying this approach to a 'staircase' of lakes at increasing altitudes in one region, or preferably in a single well-defined locality, a RSL curve can be reconstructed; often, this is more precise than the raised beach approach.

To date, Antarctic RSL curves are limited to the ice free regions of the Scott Coast and Victoria Land Coast (Hall et al., 2004), the Vestfold Hills (Zwartz et al., 1998), Larsemann Hills (Verleyen et al., 2005; Hodgson et al., 2009), and Lützow Holm Bay (Miura et al., 1998) in East Antarctica. On the Antarctic Peninsula, RSL curves and sea-level constraints exist for Alexander Island (Roberts et al., 2009), Marguerite Bay, and the South Shetland Islands (Bentley et al., 2005; Fretwell et al., 2010; Hall, 2010; Watcham et al., 2011). There are, however, no RSL curves, and only a limited number of RSL constraints, for the north-eastern Antarctic Peninsula region (e.g. Ingólfsson et al., 1992; Hjört et al., 1997) where the recent warming trend is most marked (Steig et al., 2009).

In this paper, we construct a RSL curve for Beak Island, located in Prince Gustav Channel on the north-eastern side of the Antarctic Peninsula, using a combination of geomorphological evidence of former marine limits and radiocarbon-dated marine-freshwater transitions in three isolation basins. We compare our reconstruction with a suite of glacio-isostatic adjustment (GIA) models, and determine which model is best constrained by the geological field evidence.

1.1. Site description

Beak Island (63 °36′S, 57 °20′W) is the partially submerged periphery of an inactive volcanic caldera situated in Prince Gustav Channel between Vega Island and the Tabarin Peninsula (Fig. 1), on the north-western side of the Weddell Sea Embayment. The island is composed of Miocene volcanic rocks, mainly porphyritic basalt, hyaloclastites and pillow lavas belonging to the James Ross Volcanic Island group (Bibby, 1966). The geology of the Antarctic Peninsula and James Ross Island has been described by several authors (see Ingólfsson et al., 1992, and references therein). Beak Island exhibits geomorphological evidence of former marine limits, and a series of isolation lakes and ponds (Figs. 2 and 3). Beak Lake 1 (all lake names are unofficial) is the largest and deepest lake on Beak Island; it has a diameter of c. 400 m and maximum water depth of 24 m, and occupies a depression likely created by a secondary eruption vent. It is fed by catchment snowmelt via multiple small braided meltwater streams and wet seepages, which are colonised by thick moss. The lake drains into a series of small ponds including Beak Lake 2 and Beak Lake 3, which are 4 m and 1 m deep, respectively. Beak Lake 2 is an irregularly shaped lake (c. 200 × 300 m) and Beak Lake 3 is a shallow pond (c. 100 × 80 m) just 30 m from the coast. Beak Lake 1 and Beak Lake 2 are freshwater lakes, with their biota dominated by benthic microbial mats and mosses, while Beak Lake 3 is fed by fresh meltwater but has an elevated salinity due to the influence of sea spray from the nearby coast. The limnology and a brief description of the geomorphological setting of these lakes is described in Sterken et al. (in press).

2. Methods

The locations and altitudes of the key geomorphological features, including sill heights of the lakes and ponds and the present day marine limit were determined using a Trimble 5700 GPS. All measured altitudes were referenced to the WGS 84 reference ellipsoid and corrected using the EGM96 geoid model.

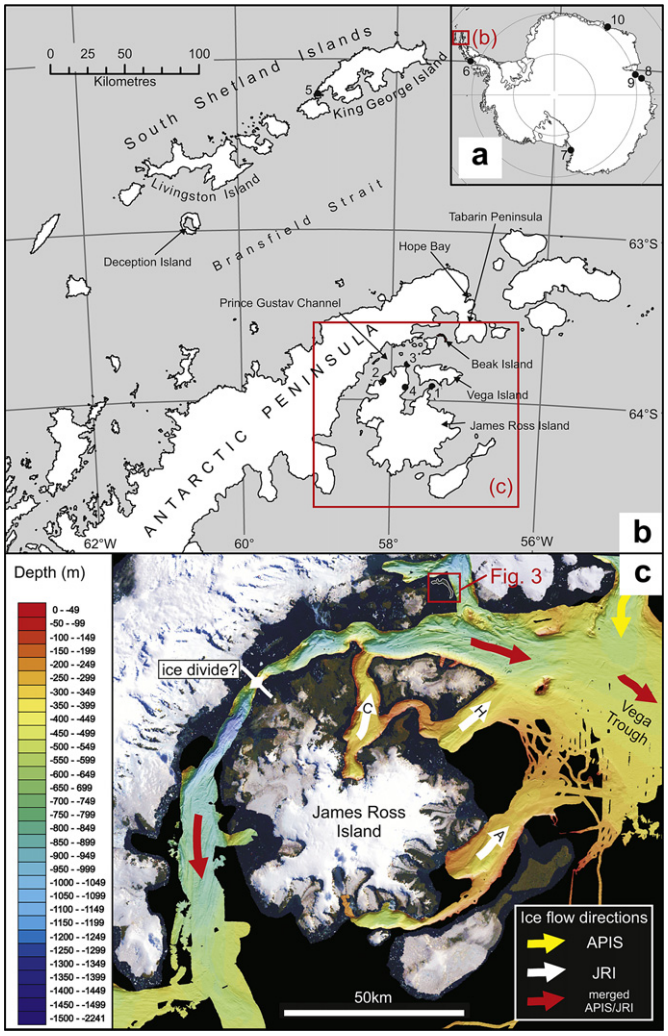

Fig. 1. (a) and (b) Location map showing Beak Island and other sites in the northern Antarctic Antarctic Peninsula region where relative sea-level data are available. These are (1) The Naze, James Ross Island (Hjört et al., 1997), (2) Brandy Bay, James Ross Island (Hjört et al., 1997), (3) Cape Lachman, James Ross Island (Ingólfsson et al., 1992), (4) St. Martha Cove (Ingólfsson et al., 1992), (5) South Shetland Islands (Bentley et al., 2005; Fretwell et al., 2010; Hall, 2010; Watcham et al., 2011). Other regions where RSL curves are available in Antarctica are shown on the inset map as (6) Marguerite Bay (Bentley et al., 2005), (7) Victoria Land and Scott Coasts (Hall et al., 2004), (8) Vestfold Hills (Zwartz et al., 1998), (9) Larsemann Hills (Verleyen et al., 2005), (10) Lützow Holm Bay (Miura et al., 1998). (c) Swath bathymetry data from around James Ross Island (JRI) showing the location of Beak Island in the context of a major former outlet of the Antarctic Peninsula Ice Sheet (APIS) and ice flow directions of the former APIS and JRI ice sheets (adapted and reproduced with permission from Johnson et al. (in press), which synthesises data from RVIB Nathaniel B Palmer cruises NBP0003 and NBP0107; RRS James Clark Ross cruise JR71; RVIB Nathaniel B Palmer cruises 0201, 0502 and 0602 and HMS Endurance surveys).

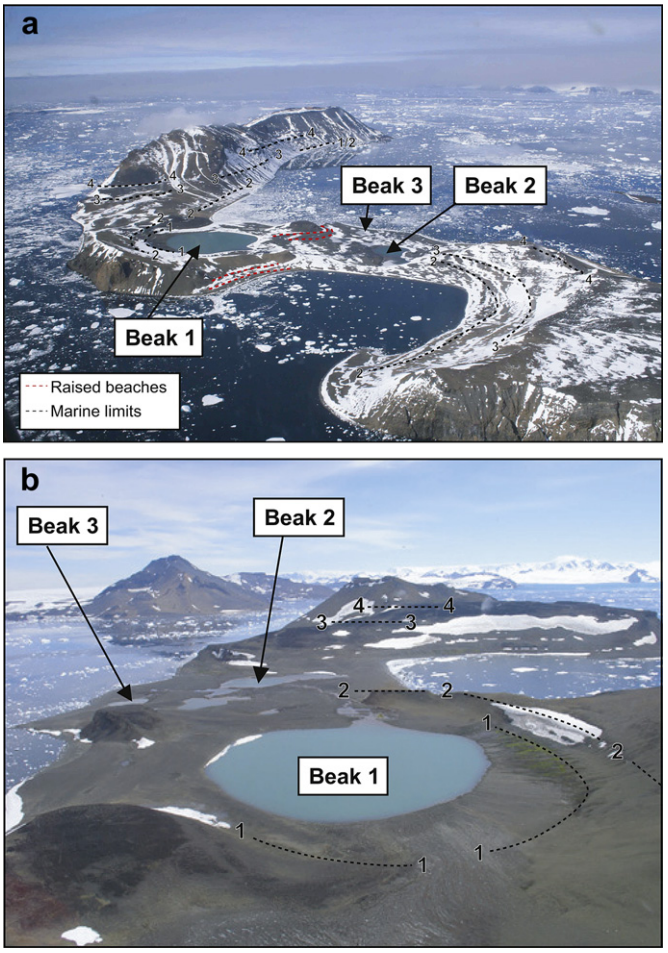

Fig. 2. Oblique aerial photographs of Beak Island showing isolation basins and former marine limits (a) looking approximately south east; (b) looking approximately west. Marine limits 1–4 shown are as follows: (1) Holocene age; (2) late Quaternary age (uncertain); (3, 4) Quaternary or pre-Quaternary.

The CGIS statistical accuracy assessment is better than ±10 cm for all the results; latitude and longitude determinations are generally better than ±1–3 cm, and altitudes ±3–5 cm with a few outliers up to 10 cm. The location and lithological composition of boulders >50 cm in diameter within the most significant 'boulder fields' was also mapped (Fig. 3).

Sediment cores were taken at depths of 20 m, 4 m and <1 m in Beak Lakes 1, 2 and 3 respectively using a UWITEC gravity corer and a Livingstone corer (Livingstone, 1955). Flocculent surface sediments were sectioned at 0.5 cm resolution in the field and duplicate Livingstone core sections from Beak Lake 1 were retained intact for non destructive core scanning.

To identify marine to freshwater transitions, cores were analysed for wet density, dry weight, organic and carbonate content by % weight loss on ignition (Dean, 1974), C/N ratio (Meyers and Teranes, 2001), and volume specific magnetic susceptibility using a Bartington 1 ml MS2G sensor. Diatoms were prepared following Renberg (1990), with absolute abundances calculated following Battarbee and Kneen (1982), Diatom counting methods and taxonomy followed Sterken et al. (in press) and diatom assemblages were zoned using stratigraphically constrained cluster analysis (CONISS, Grimm, 1987). Diatom transition zones were defined as the periods in which marine taxa start to disappear, brackish-water taxa peak and freshwater taxa start to appear. These differ slightly from the CONISS transition zones because the time needed for the freshwater community to fully stabilise (indicated by pioneer species decreasing in abundance) is influenced by other factors such as the depth and volume of the lakes.

A chronology for the sediment cores, focussed on dating the marine to freshwater transitions, was established by AMS radiocarbon (^{14}C) dating organic macrofossil remains of moss macrofossils preserved in the Beak Lake 1 sediment core of the species *Cratoneuropsis Chilensis* (also referred to as *Cratoneuropsis relaxe* (*subsp. minor*) (aquatic moss) (Ochyra, 2008, Ochyra pers. comm.), large, 1–2 mm long, cyanobacterial mat fragments from Beak Lakes 2 and 3 and fine-very fine cyanobacterial mat-derived deposits in Beak Lake 1. Bulk (inorganic) sediments were also dated where no

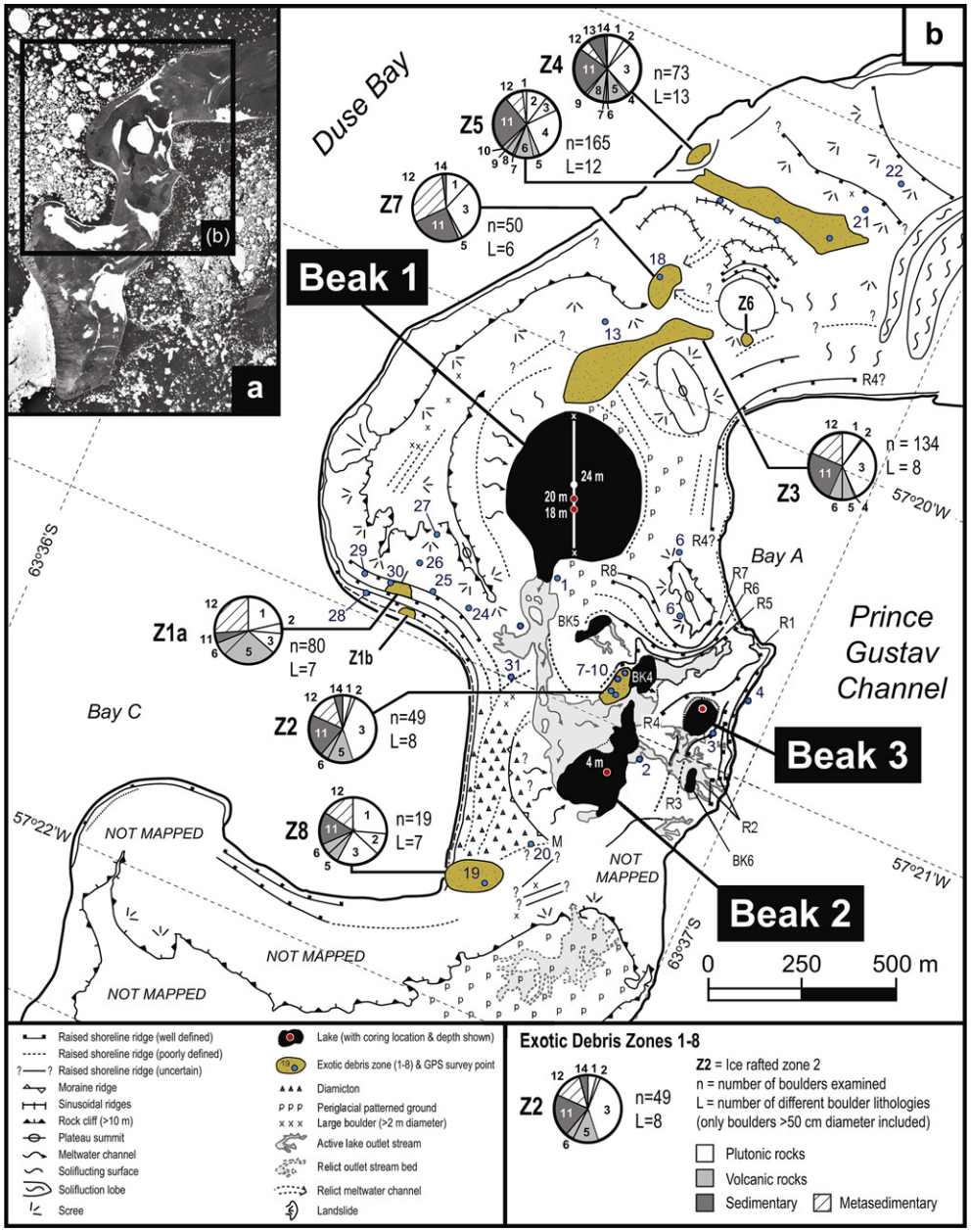

Fig. 3. (a) Aerial photograph of Beak Island; (b) Summary geomorphological map of Beak Island showing the three studied isolation basins (Beak Lakes 1–3), other shallow water bodies Beak Lakes 4–6 and position and summary lithological pie-charts for the main zones of 'exotic' debris on Beak Island. Lithological key: 1 = pink granite; 2 = granodiorite; 3 = diorite; 4 = sheared diorite; 5 = andesite; 6 = porphyritic basalt; 7 = pillow lava; 8 = hyaloclastite; 9 = red ashstone; 10 = green ashstone; 11 = massive mudstone/siltstone; 12 = meta-sedimentary (laminated meta-mudstone/siltstone & gneiss); 13 = mudstone shale; 14 = sandstone. (For interpretation of the references to colour in this figure legend, the reader is referred to the web version of this article.)

moss macrofossils or bulk cyanobacterial mat deposits were available. Paired cyanobacterial mat-moss macrofossil and moss macrofossil-bulk sediment dating was carried out to check for consistency (Table 2).

Moss macrofossils were hand-picked from frozen bulk material, after overnight defrosting at 5 °C, immersed in ultra-pure (18.2 m Ohm) water, sealed and placed an ultrasonic bath for an hour, refrozen and stored. Samples were sent frozen to Scottish Universities Environmental Research Centre (SUERC) and Beta Analytic (Miami, Florida) for accelerator mass spectrometry (AMS) radiocarbon dating. SUERC-samples were heated in 2 M HCl (80 °C for 8 h), rinsed in deionised water, until all traces of acid had been removed, and dried in a vacuum oven. Inorganic sand and rock fragments in samples SUERC-12947, 12574, 12575, 12576, 12577 were removed by sieving/hand-picking and set aside from finer organic bearing material before combustion. Further moss samples dated by Beta Analytic (BETA 288864–67) were leached with a 0.5–1.0 M HCl bath to remove carbonates, heated to 70 °C for 4 h. Leaching was repeated until no carbonate remained, followed by rinsing to neutral 20 times with deionised water, samples were then placed in 0.5–2% solution of NaOH for 4 h at 70 °C and rinsed to neutral 20 times with deionised water. The process was repeated until no additional reaction (typically indicated by a coloration change in the NaOH liquid) was observed. Samples were then leached again with a 0.5–1.0 M HCl bath to remove any CO_2 absorbed from the atmosphere by the NaOH soakings and to ensure

Table 1
GPS surveys of marine limits, isolation basin sills and present high water mark on Beak Island (* indicates altitudes that are equal to the MSL altitude minus the height of the antenna on the tripod).

Site	Latitude	Longitude	WGS 84 alt (m)	Geoid alt (m)	MSL alt (m)	Corrected MSL alt (m)*	Alt (m) above present HWM
Earlier (pre?) Quaternary marine limit	−63 ° 36′ 49.7725″	−57 ° 20′ 36.6677″	47.664	22.55	25.11	25.01	25.31
Holocene marine limit	−63 ° 36′ 47.5462″	−57 ° 20′ 26.2073″	38.163	22.55	15.61	14.91	15.21
Beak 1 sill	−63 ° 36′ 39.2349″	−57 °20′ 39.5940″	34.372	22.56	11.81	10.95	11.25
Beak 2 sill	−63 ° 36′ 51.5235″	−57 ° 21′ 03.9619″	25.802	22.55	3.30	2.365	2.665
Beak-3 sill	−63 ° 36′ 55.9714″	−57 ° 20′ 54.2506″	23.928	22.54	1.39	0.515	0.815
High water mark	−63 ° 36′ 57.7942″	−57 ° 20′ 45.6882″	23.017	22.54	0.48	−0.3	0

initial carbonate removal was complete, then dried at 70 °C in a gravity oven for 8–12 h.

Dates are reported as conventional radiocarbon years BP (^{14}C yr BP)+/−1σ, and in years AD for 'modern' moss sample ages calibrated in CALIBomb using the SH1 dataset, a compilation of Southern Hemisphere datasets (Hua and Barbetti, 2004; Reimer et al., 2004b). They are also referred to as calibrated years BP (cal yr BP relative to AD 1950) with calibrations performed in CALIB V. 6.0 (Reimer and Reimer, 2011) using the SHCal04.14C atmosphere dataset (McCormac et al., 2004; Reimer et al., 2004a) for freshwater samples, the MARINE09 calibration curve (Reimer et al., 2009) for marine samples, and a mixed MARINE09–SH04. curve (50% marine) for samples at marine-lacustrine transitions. The absolute percentage of modern carbon (pMC) data were corrected according to ^{13}C/^{12}C isotopic ratios from measured pMC, where the "modern" (i.e., AD 1950) pMC value is 100 and the present day (2010) pMC value is 107.5. For the marine samples, dates were corrected for the marine reservoir effect by using ΔR value of 880+/−50 years based on the nearest measurements of the pre-1950 AD marine reservoir effect at Hope Bay which consists of penguin bones from animals consumed at a refuge constructed during the unplanned winter of Dr Otto Nordenskold's 1903 Expedition that have been dated at 1280+/−50 ^{14}C yr BP (LU3101) (Björck et al., 1991b). The 'classical' radiocarbon age-depth modelling presented in Fig. 4 was undertaken using CLAM software (http://www.chrono.qub.ac.uk/blaauw/clam.html; (Blaauw, 2010)), with probability distributions for modern 'bomb'-carbon influenced, and mixed marine/freshwater samples generated and imported from OxCal V.4 (www.c14.arch.ox.ac.uk/oxcal.html; (Bronk Ramsey, 2001)); all median calibrated ages and ranges quoted are 2σ error. To assist in future with tracking reservoir correction and calibration procedures, ages cited in the text from this point onwards have not been rounded. For radiocarbon ages with 1σ errors less than ±50 years, rounding of ages to the nearest five years samples is normally recommended. Where 1σ errors are greater than ±50 years, ages are normally rounded to the nearest 10 years.

3. Results

3.1. Geomorphology

At least three former marine limits were identified from field-based geomorphological observations and mapping (Fig. 3): (1) a marine surface at 74–94 m (±5 m; measured using a hand-held Garmin Quad sensor GPS), which possibly corresponds to the pre-Quaternary limit found on James Ross Island (Hjört et al., 1997) and the South Shetland Islands (Sugden and John, 1973); (2) a Quaternary or pre-Quaternary surface at 25.0 m; and (3), a uniform erosion surface which marks the Holocene marine limit at 14.91 m. The 'staircase' of lakes and ponds on the island are all below the 14.91 m marine limit, and therefore became isolated from the sea during the Holocene. The altitudes of their retaining sills are given in Table 1. We did not correct the altitudes of these Holocene features for tectonic processes because estimates are in the order of 'several hundred metres in the past few million years' (Smellie J., pers. comm.), equating to <1 m elevation change over the Holocene.

Eight prominent zones 'exotic' debris zones with numerous boulders >50 cm were found around the lakes at altitudes ranging from c. 8–50 m.a.s.l. (Fig. 3). The boulders have a variety of sizes, shapes, and 'exotic' lithologies. Their random patchy, yet well-constrained distribution on and below previously elevated shoreline ridges (Z1/2; Fig. 3) or across swathes of the central area of the island (Z3-7), which would have once been submerged, suggests deposition through ice-rafting of glacial debris by icebergs.

3.2. Chronology

Radiocarbon dates indicated that the lake sediments are Holocene in age with median basal calibrated ages of 10,612 cal yr BP (Beak Lake 1), 4166 cal yr BP (Beak Lake 2) and 2013 cal yr BP (Beak Lake 3) (Table 2). The surface moss dated in Beak Lake 1 returned a near-present day or 'modern' percentage modern carbon (pMC) value, suggesting no reservoir effects prior to 1950. In Beak Lake 2, the median calibrated age of the microbial mat surface sample was 389 cal yr BP, which suggests mixing of the surface sediments has occurred in this shallow lake. Similarly, in Beak Lake 3, some disturbance of the upper few centimetres of sediment may have occurred, as there is a modern aged moss sample at 8.5 cm depth, while the surface (bulk sediment/microbial mat influenced) sample has a median calibrated age of 495 cal yr BP (Table 2).

As live microbial mat communities were observed in the Beak Lakes 2 and 3 surface sediment cores, we have assumed a zero age for the reworked surface deposits in these lakes in our age models. The absence of a local reservoir effect in the much deeper Beak Lake 1, supports our interpretation that non-zero ages in lakes Beak Lakes 2 and 3 are due to wind-induced shallow water mixing. Further, there are no obvious sources of old carbon in catchments of the present day lakes: no glacier remains in the only cirque on the island, and there were no persistent/perennial snow patches around the lakes when visited.

In general, radiocarbon ages from Beak Lakes 1–3 were in stratigraphic order with the exception of anomalously young ages at 15.5 cm and 32.5 cm in Beak Lake 1. Although all macrofossil samples for dating were taken from the central part of the cores, we cannot rule out the possibility that these anomalous ages could have been the result of translocation of some surface moss fragments from the dense, 5 cm thick moss layer in Beak Lake 1, which required a considerable amount of effort to penetrate during coring. However, in this study, and in our recent studies on the South Shetland Islands (Watcham et al., 2011), we have observed that some radiocarbon ages from aquatic mosses adjacent to visible

Table 2
Radiocarbon dates for the Beak Island lake sediment cores. Calibration of ^{14}C age data is as follows: calibration models: A = CALIBomb SH1, a compilation of Southern Hemisphere datasets ((Hua and Barbetti, 2004); http://calib.qub.ac.uk/CALIBomb/), using the absolute percentage of modern carbon (pMC) data, corrected according to $^{13}C/^{12}C$ isotopic ratios from measured pMC, where 'modern' is 1950 AD and 100 pMC, and 'present day' is defined as 2010 and 107.5 pMC; B = SHCal04.14C atmosphere (McCormac et al., 2004); http://calib.qub.ac.uk/calib/calib.html) where cal yr BP = yr before 1950 AD; C = SHCal04.14C atmosphere 50% atmosphere 50% MARINE09 mixed model; D = Intcal09.^{14}C Marine with ΔR set to 880+/−50 to account for the local marine reservoir offset – see text (Reimer et al., 2009). * indicates absolute pMC. Probabilities with a total sum >0.95 are shown; 'x' = age omitted from age-depth model due to ages being out of sequence or reworking of older sediment; # = ages adjacent to visible volcanic ash layers volcanic ash layers were omitted from age models as they appear to give ages that are compromised, either due to their relatively low organic content, reworking following catchment, marine sediment disturbance, localised disturbance of atmospheric carbon equilibrium by volcanic activity, or translocation of younger material during coring.

Lab/Publication Code	Core ID & depth	Stratigraphic depth (cm)	Summary description	Carbon source	Marine/ Lacustrine	Carbon content (wt %)	$\delta^{13}C_{VPDB}$ (‰)	pMC/^{14}C enrichment (% modern ± 1σ)	Conventional radiocarbon age (years BP ± 1σ)	2σ calibrated age data (A = yr AD; B–D = cal yr BP)			
										Min.–Max.	Rel. Prob.	Median prob.	Age Model
Beak Lake 1													
SUERC-12385	BK1E:0–1	0–1	Fine strands aquatic moss *Cratoneuropsis chilensis*	Macrofossil	Lacustrine	44.2	−32.4	108.6 ± 0.5 107.9 ± 0.5*	Modern	**>2004 AD** or 1957–1958	1.00 0.00	**>2004 AD** 1958 AD	A Ax
BETA-288864	BK1E:2.5	2.5–3	Fine strands aquatic moss *Cratoneuropsis chilensis*	Macrofossil	Lacustrine	26.8	−26.5	122.2 ± 0.5 122.5 ± 0.5*	Modern	1982–1986 1961–1962	0.86 0.11	1984 AD 1961 AD	A
BETA-288865	BK1E:4	4–4.5	Fine strands aquatic moss *Cratoneuropsis chilensis*	Macrofossil	Lacustrine	43.0	−27.1*	94.1 ± 0.5	490 ± 40	451–545	0.98	505	B
BETA-288866	BK1E:8.5	8–8.5	Fine strands aquatic moss *Cratoneuropsis chilensis*	Macrofossil	Lacustrine	4.2	−25.4	81.4 ± 0.5	1650 ± 50	1368–1607	1.00	1477	B
BETA-288867	BK1E:12	12–12.5	Olive green fine organic mud/mat	Mat (TOC)	Lacustrine	2.8	−28.4*	79.8 ± 0.4	1810 ± 40	1557–1742 1753–1811	0.90 0.10	1663	B
SUERC-12394	BK1E:15.5	15.5–16	Greenish grey laminated fine organic mud	Mat (TOC)	Lacustrine	1.4	−26	82.3 ± 0.4	1563 ± 35	1311–1424 1457–1516	0.78 0.19	1390	B #
Not analysed	BK1E:15.5	15.5–16	Very fine strands aquatic moss *Cratoneuropsis chilensis*	Macrofossil	Lacustrine	*Insufficient material for AMS dating; 2 attempts*							−x
SUERC-12395	BK1E:31	31–32	Olive green fine mud/light grey clay laminations	Mat (TOC)	Lacustrine	9.3	−29.8	75.1 ± 0.3	2305 ± 35	2153–2277 2289–2344	0.69 0.32	2235	B
SUERC-12386	BK1E:32-33	32–33	Fine strands aquatic moss *Cratoneuropsis chilensis*	Macrofossil	Lacustrine	30.0	−28.9	87.2 ± 0.4	1101 ± 35	914–1015 1023–1055	0.87 0.13	957	B #
SUERC-12396	BK1E:34	34–35	Consolidated medium-dark olive green mud/mat	Mat (TOC)	Lacustrine	11.4	−31.4	74.7 ± 0.3	2345 ± 35	2297–2355 2157–2265	0.54 0.46	2307	B
SUERC-12397	BK1E:43.5	43–44	Light grey-olive green fine organic mud/mat	Mat (TOC)	Lacustrine	6.7	−30.4	69.4 ± 0.3	2940 ± 35	2918–3160	0.95	3018	B
SUERC-12398	BK1E:46	46–47	Light grey-olive green fine organic mud/mat	Mat (TOC)	Lacustrine	4.0	−29.3	66.5 ± 0.3	3280 ± 35	3370–3511 3518–3557	0.89 0.11	3441	B
SUERC-12401	BK1E:55	55–56	Light grey-olive green fine organic mud/mat	Mat (TOC)	Lacustrine	4.1	−29.9	60.4 ± 0.3	4048 ± 35	4384–4571	0.96	4473	B
SUERC-12402	BK1E:59	59–60	Light grey-olive green fine organic mud/mat	Mat (TOC)	Lacustrine	3.0	−30.2	58.2 ± 0.3	4346 ± 35	4816–4972	0.97	4857	B
SUERC-12403	BK1E:73.5	73–74	Medium-light olive green fine organic mud/mat	Mat (TOC)	Transition end	9.6	−26.7	47.3 ± 0.2	6010 ± 36	6674–6888	1.00	6783	B
SUERC-12564	BK1D:8.5	73–74	Medium-light olive green fine organic mud/mat	Mat (TOC)	Transition end	8.7	−27.8	46.8 ± 0.2	6098 ± 35	6781–7001	0.99	6890	B
SUERC-12404	BK1E:78.5	78–79	Dark greenish grey/black fine organic mud	Bulk (TOC)	Transition start	3.1	−22.4	43.2 ± 0.2	6735 ± 35	6797–7088	0.97	6944	C
SUERC-12565	BK1D:14.5	79–80	Dark greenish grey laminated organic mud	Bulk (TOC)	Transition start	1.2	−22.5	39.8 ± 0.2	7393 ± 36	7508–7672	1.00	7596	C
SUERC-12943	BK1D:38.5	103–104	Dark greenish grey laminated fine organic mud	Bulk (TOC)	Marine	0.3	−21.9	25.7 ± 0.2	10901 ± 53	10.734–11,173	1.00	10,993	D x
SUERC-12566	BK1D:43.5	108–109	Laminated organic mud with coarse sand/silt and clay	Bulk (TOC)	Marine	0.2	−21.5	30.2 ± 0.2	9626 ± 48	9255–9532	1.00	9418	D
SUERC-12944	BK1D:64.5	129–130	Clay rich black volcanic silty sand (reworked?)	Bulk (TOC)	Marine	0.2	−20.6	26.2 ± 0.2	10,752 ± 62	10,578–11,069	1.00	10,796	D #
SUERC-12945	BK1D:75.5	140–141	Clay rich black volcanic silty sand (airfall?)	Bulk (TOC)	Marine	0.2	−21.2	28.3 ± 0.2	10,147 ± 46	9873–10,238	1.00	10,090	D
SUERC-12567	BK1D:101	166–167	Dark greenish grey/black coarse sand and silt/clay bands	Bulk (TOC)	Marine	0.3	−21.5	26.6 ± 0.2	10625 ± 54	10,461–10,892	1.00	10,612	D

Beak Lake 2													
SUERC-12568	BK2A:0-1	0–1	Orange microbial mat (living) layer	Mat (TOC)	Lacustrine	6.8	−14.7	95.9 ± 0.4	339 ± 35	300–461	1.00	389	B
Not analysed	BK2A: 16-17	16–17	*Cratoneuropsis chilensis* 'leaves' & microbial mat	Macrofossil	Lacustrine	*Insufficient material for AMS dating; 2 attempts*							-x
SUERC-12387	BK2A:50-51	50–51	*Cratoneuropsis chilensis* 'leaves' & microbial mat	Macrofossil	Lacustrine	49.4	−21.6	95.1 ± 0.4	400 ± 35	324–415 426–496	0.52 0.46	410	B
SUERC-12388	BK2A:70-71	70–71	*Cratoneuropsis chilensis* moss in microbial mat	Macrofossil	Lacustrine	22.3	−19.5	84.2 ± 0.4	1377 ± 35	1178–1300	1.00	1256	B
SUERC-12391	BK2A:72-73	72–73	*Cratoneuropsis chilensis* moss in microbial mat	Macrofossil	Lacustrine	46.4	−25 (est)	84.8 ± 0.4	1329 ± 35	1166–1289 1124–1163	0.89 0.08	1217	B
SUERC-12569	BK2B:43-44	136–137	Laminated organic mat/mud	Mat (TOC)	Lacustrine	6.1	−16.9	74.4 ± 0.3	2374 ± 35	2301–2460 2178–2244	0.80 0.19	2338	B
SUERC-12946	BK2B:55-56	148–149	Dark-light olive green mat	Mat (TOC)	Transition end	3.8	−16.1	70.8 ± 0.3	2780 ± 35	2753–2888	0.97	2821	B
SUERC-12570	BK2B:66-67	159–160	Black fine organic mud	Bulk (TOC)	Transition start	1.7	−17.2	63.6 ± 0.3	3632 ± 35	3055–3335	1.00	3191	C
SUERC-12947	BK2C:53-54	240–241	Black fine-medium organic mud/coarse sand	Bulk (TOC)	Marine	0.7	−15.5	53.7 ± 0.2	4990 ± 36	3975–4360	1.00	4166	D
Beak Lake 3													
SUERC-12574	BK3A:0-1	0–1	Olive grey/green massive/ structureless mat and mud	Mat (TOC)	Lacustrine	2.5	−13.9	94.3 ± 0.4	471 ± 35	448–533 336–357	0.94 0.06	495	B x
SUERC-12392	BK3A:8-9	8–9	*Cratoneuropsis chilensis* 'leaves' & microbial mat	Macrofossil	Lacustrine	31.1	−23.5	122.2 ± 0.5 121.2 ± 0.5*	Modern	1983–1986 1960–1989	0.75 1.00	1984 AD 1975 AD	A A
SUERC-12575	BK3A:28-29	28–29	Olive grey massive/structureless mud/mat	Mat (TOC)	Lacustrine	4.9	−12.6	83.5 ± 0.4	1453 ± 35	1271–1372	1.00	1311	B
SUERC-12576	BK3A:44-45	44–45	Light grey/black massive mat	Mat (TOC)	Transition end	9.4	−12.3	81.1 ± 0.4	1686 ± 35	1411–1614	1.00	1524	B
SUERC-12577	BK3A:48-49	48–49	Dark grey/black silt, fine sand and structureless mat	Mat (TOC)	Shallow brackish	5.6	−13.6	79.9 ± 0.4	1806 ± 35	1552–1741	0.95	1658	B
SUERC-12948	BK3A:58-59	58–59	Dark grey/black silt and fine structureless volcanic sand	Bulk (TOC)	Shallow marine	1.4	−12.7	71.6 ± 0.3	2684 ± 35	1896–2127 2712–2844	1.00 0.98	2013 2755	C B x

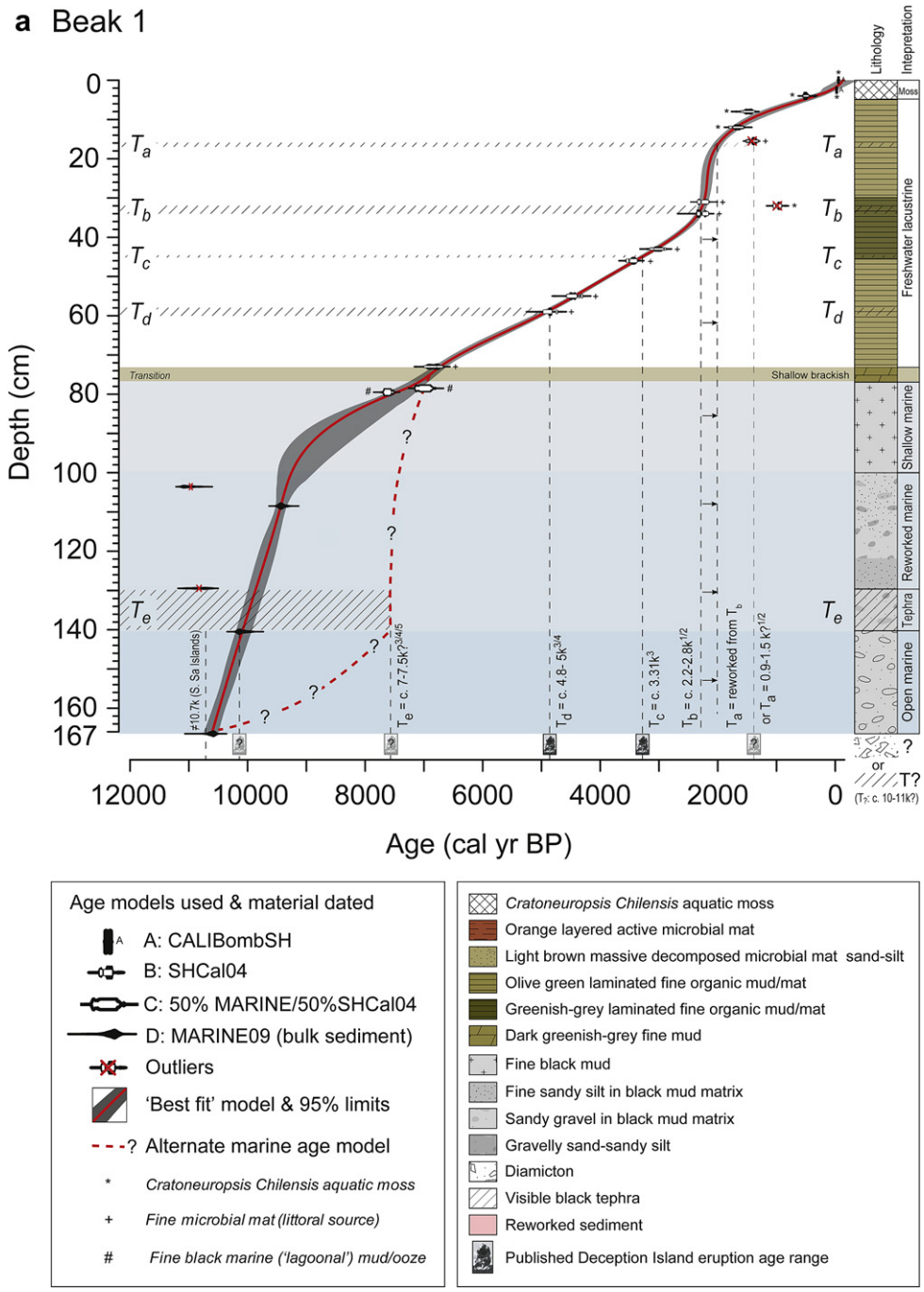

Fig. 4. Stratigraphic age-depth plots undertaken in CLAM (Blaauw, 2010) and lithology for (a) Beak Lake 1 and (b) Beak Lake 2 and (c) Beak Lake 3. CLAM settings: smooth spline (smoothing 0.3); 1000 iterations weighted by calibrated probabilities at 95% confidence ranges and resolution 1 year steps. CLAM output statistics: (a) Beak Lake 1: 0–166 cm; 350 models with age reversals were removed; −log goodness of fit = 139.09; 95% confidence range 126–1006 years, average 306 years; (b) Beak Lake 2: 0–240 cm; − log goodness of fit = 14.38; 95% confidence range 2–346 years, average 260 years; (c) Beak Lake 3: 8–58 cm; − log goodness of fit = 8.78; 95% confidence range 32–248 years, average 144 years. T_a, T_b, T_c, T_d, and T_e are prominent tephra layers in the core which were used to provide independent chronological constraints. Tephra references: 1 = Björck et al. (1991a); 2 = Hodgson et al. (1998); 3 = Willmott et al., (2006); 4 = Lee et al. (2007); 5 = Watcham et al. (2011). Deception Island 1967 eruption thumbnail photo by D. Borthwick in Clapperton (1969).

volcanic ash (tephra) layers appear to be compromised, either by reworking following catchment disturbance and/or due to possible changes in local-regional atmospheric ^{14}C equilibrium associated with large volcanic eruptions. As the influence of the latter is relatively poorly understood in this region, we have excluded these two radiocarbon age outliers, as they are adjacent volcanic ash deposits T_a and T_b (Fig. 4a). Independent constraints on the Beak Lake 1 chronology are provided by the regional tephrochronology to be described in a forthcoming paper.

3.3. Isolation evidence and dates

In the Beak Lake 1 core, the basal marine sedimentary unit is overlain by up to c. 70 cm of finely laminated 'organic-rich' mud

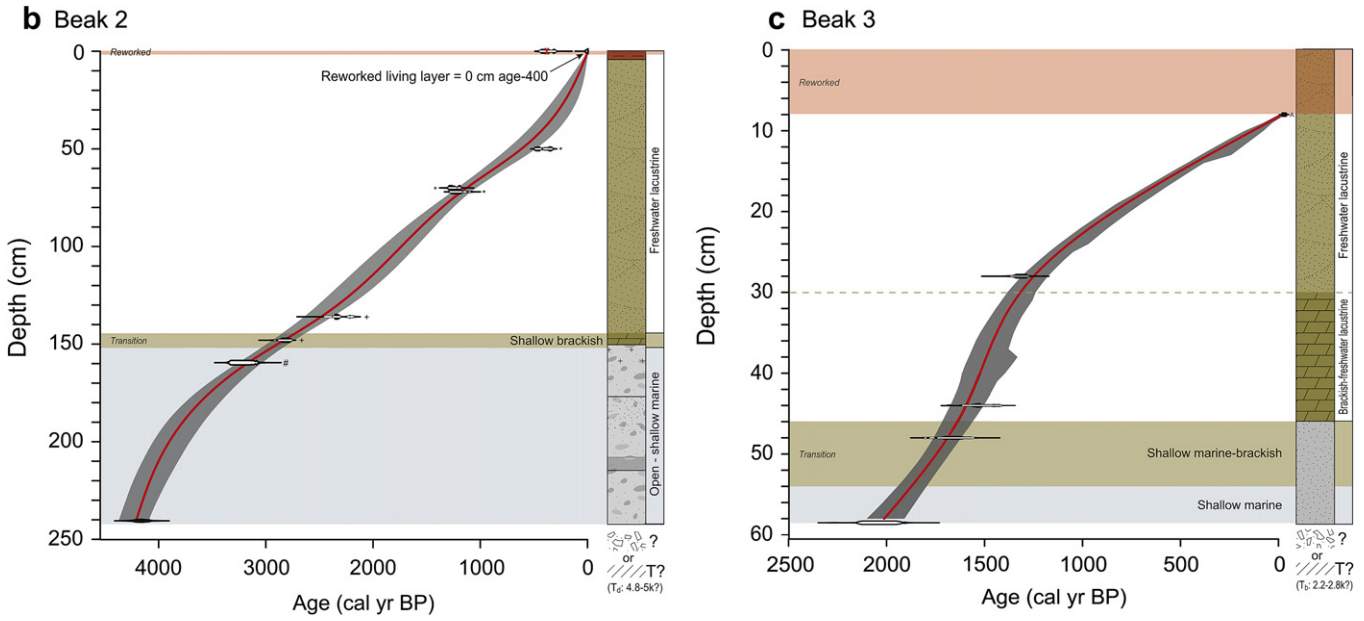

Fig. 4. (*continued*).

and clay/silt (Fig. 4a). The lithology of the Beak Lake 2 and 3 cores is broadly similar, with marine sediments consisting of dark grey to black organic muds with varying degrees of sand and silt, overlain by freshwater sediments, which consist predominantly of microbial mats in varying states of decay, and intercalated fine organic muds (Fig. 4b and c).

Isolation of the lakes was identified by clear shifts in the sedimentological and geochemical data, and clear transitions from marine to brackish, and then to freshwater diatom assemblages separated by the diatom-based cluster analyses. One marine–freshwater transition occurred in each lake.

In Beak Lake 1, the transition between marine and brackish/fresh conditions was complete by 76 cm at 6988 cal yr BP (best 'fit' age from CLAM age-depth modelling shown in Fig. 4a: age range = 6854–7161 cal yr BP). This transition was marked by a decline in wet density, and increases in organic content and the ratio of C/N (Fig. 5). The biological data show marked changes at the same time with a shift from marine diatom taxa to brackish, then freshwater taxa (Fig. 6), together with an increase in the concentration of chrysophyte cysts (Fig. 5). In Beak Lake 2, the transition was complete by 151 cm at 2920 cal yr BP (best 'fit' age from CLAM age-depth modelling shown in Fig. 4b: 2819–3019 cal yr BP), marked by increases in organic content (Fig. 5) and similar diagnostic shifts in diatom species from marine to brackish and then freshwater taxa (Fig. 6). Unlike in Beak Lake 1 the increase in total diatom concentrations occurs after the transition. In Beak Lake 3, the transition was complete by 54–46 cm (best 'fit' age range from CLAM age-depth modelling shown in Fig. 4b: 1941–1663 cal yr BP), and was identified mainly by shifts in diatom taxa (Figs. 5 and 6).

3.4. Relative sea-level reconstruction

The geomorphological evidence of a Holocene sea-level high stand at 14.91 m above present mean sea-level (Table 1), together with the isolation of Beak Lakes 1–3, and their known sill heights (Table 1) can be used to reconstruct a well-constrained RSL curve (Fig. 7). Linearly extrapolating the rate of RSL change (based on the isolation dates and sill altitudes of Beak Lake 1 and Beak Lake 2) to the Holocene marine limit on Beak Island provides a date for the high stand of c. 8750 cal yr BP, whilst a logarithmic curve based on all three isolation basins gives a date of c. 8000 cal yr BP; we consider the latter more likely as RSL fall usually follows a logarithmic function after deglaciation. The rates of sea-level fall are 3.91 mm per year from the RSL maximum at c. 8000 cal yr BP to the first isolation at 6988 cal yr BP, dropping to 2.11 mm per year between 6988 and 2920 cal yr BP, 1.63 mm per year between 2920 and 1787 cal yr BP, and finally to 0.29 mm per year during the last 1787 calibrated years. This declining rate of sea-level fall is consistent with the duration of the transitions between the disappearance of the marine diatom taxa and the appearance of the freshwater taxa (Fig. 5). The transition was shortest in Beak Lake 1 taking less than 54 years (transition 77.5–75.5 cm; ages based on minimum transition start-end 78.5–73.5 cm median ages of 6944–6890 cal yr BP; Fig. 4a), intermediate in Beak Lake 2 taking c. 60 years (from 152 to 150 cm best 'fit' ages: 2950–2890 cal yr BP; Fig. 4b) and longest in Beak-3 (from best 'fit' ages 57–47 cm: 1976–1663 cal yr BP; Fig. 4c) taking c. 313 years.

Comparing these geological constraints with a range of RSL predictions, generated using a GIA model, shows that the predictions exhibit a range of over- and under-estimates, which change through time (Fig. 7). The curve based on the ICE-5G deglaciation scenario (Peltier, 2004) predicts a local Holocene marine limit of ~35 m a.s.l. This exceeds the observed marine limit by ~20 m implying either that this model locally contains too much ice at the LGM, or that deglaciation is assumed to have taken place too late, resulting in high rates of late Holocene rebound. The curve based on the ice sheet reconstructions of Ivins and James (2005) (hereafter IJ05) shows good agreement with the isolation lake data, but only back to c. 6000 cal yr BP. This prediction falls short of the observed marine limit indicating that local LGM thicknesses are too thin, or deglaciation takes place too early in this model. The curve based on the reconstruction by Huybrechts (2002) slightly under-predicts the amount of RSL fall during the Holocene, indicating that the local LGM ice thickness is slightly too thin in this model.

The ICE-5G predictions are calculated using the VM2 earth model that was developed in conjunction with the ICE-5G deglacial history (Peltier, 2004). However, the IJ05 and Huybrechts deglaciation histories have been combined with a range of 1D (radial) Earth models, where the lithospheric thickness and

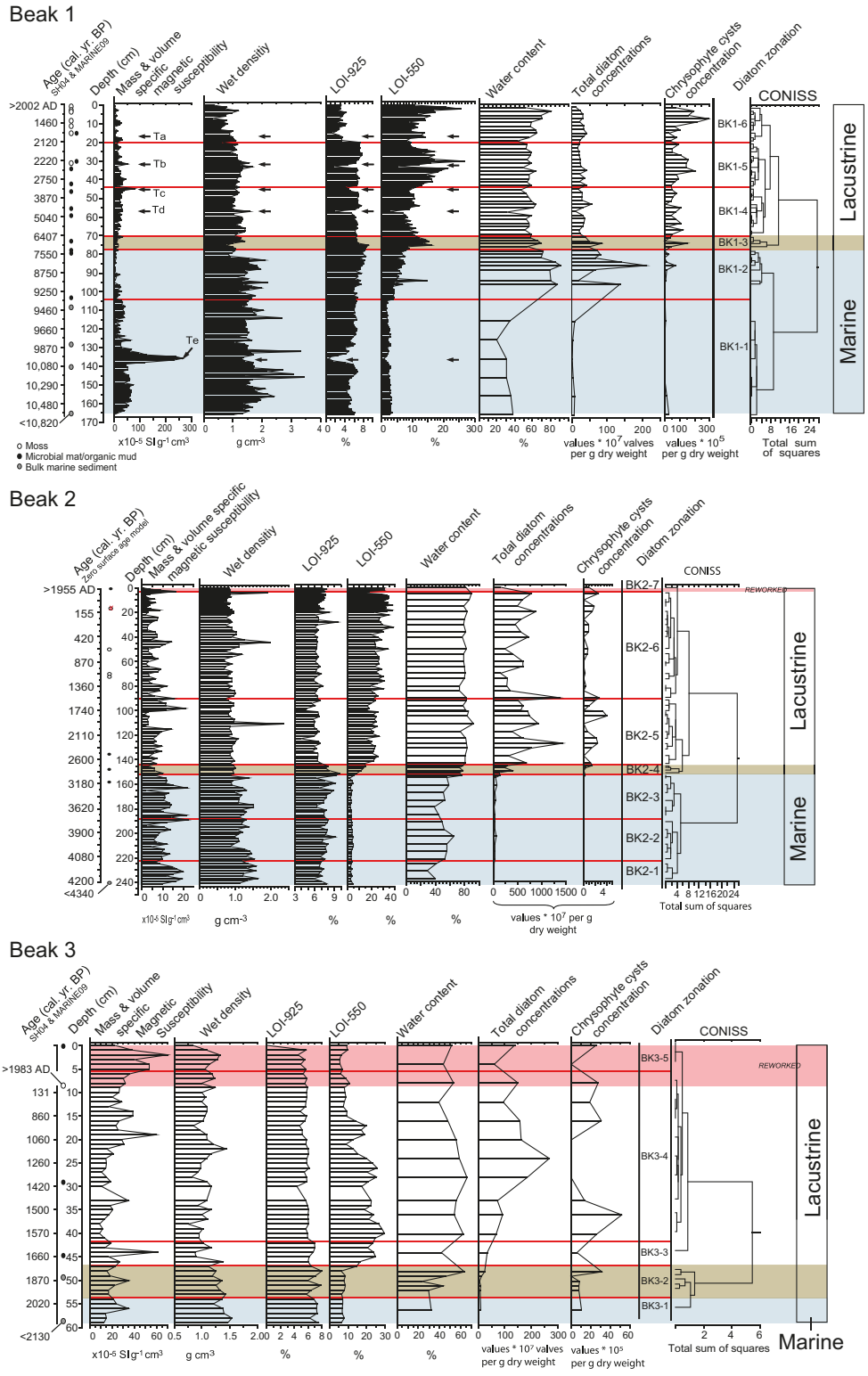

Fig. 5. Stratigraphic plots for the Beak Lake 1 sediment core (top panel), Beak Lake 2 (middle panel) and Beak Lake 3 (lower panel) showing summary sedimentological, geochemical and selected microfossil-based data. Corresponding interpolated calibrated ages are given, and depths of ^{14}C dates (Table 2) are indicated by black dots. The zonation of the core is based on a CONISS analysis of the diatom species assemblages. T_a, T_b, T_c, T_d, and T_e are visible tephra layers in the Beak Lake 1 core. Methods and descriptions of all other parameters are described in Sterken et al. (in press).

upper and lower mantle viscosities are varied, to determine the best fit to the geological data. We find that the magnitude of the high stand predicted by the Huybrechts (2002) model is strongly dependent upon the lithospheric thickness and the lower mantle viscosity, with the data preferring a relatively thin lithosphere (96 km) and a lower mantle viscosity of 10^{22} Pa s. This sensitivity to lower mantle viscosity is a reflection of the long wavelength deformation signal that is excited by the large ice mass changes

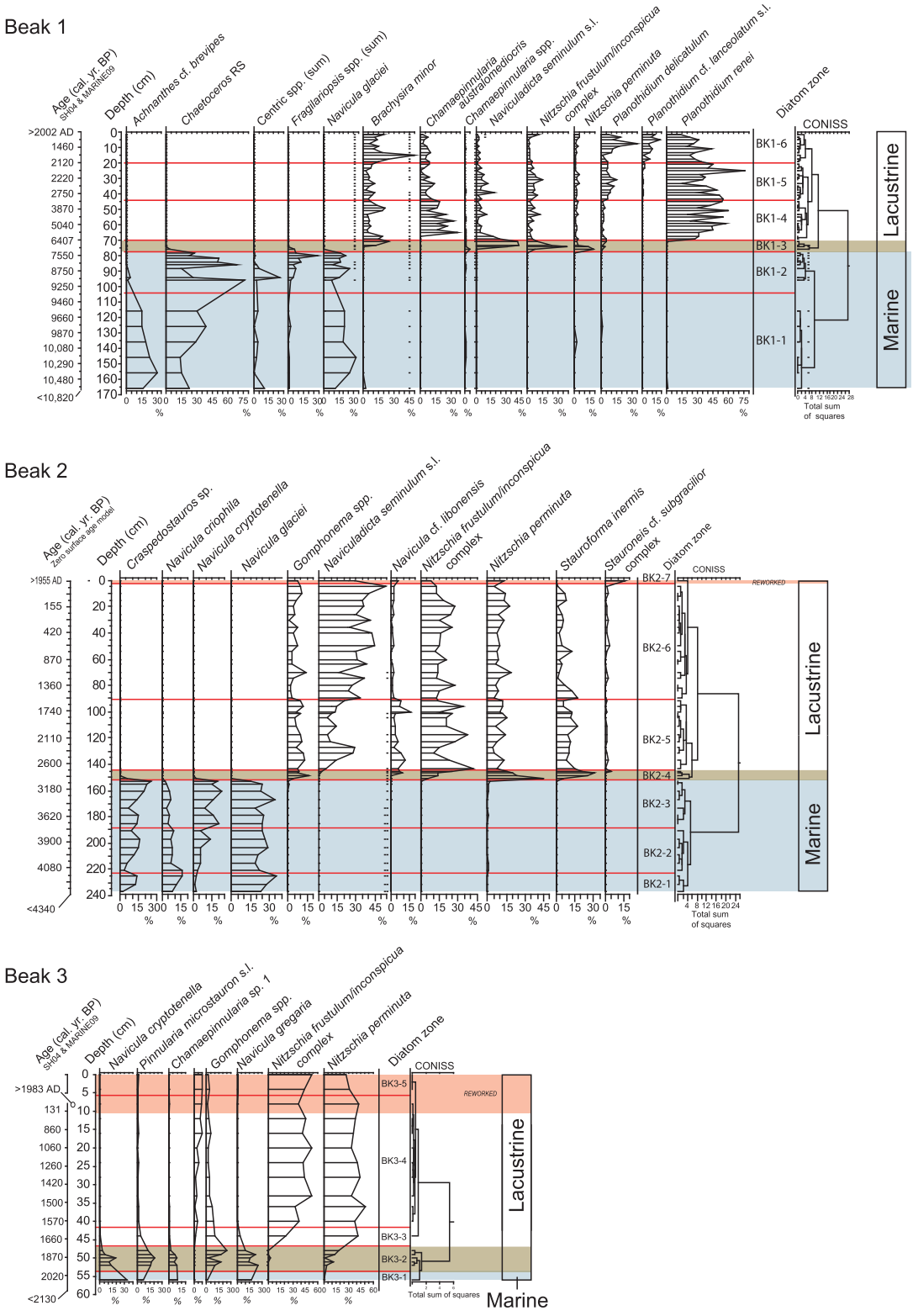

Fig. 6. Stratigraphic plots for the Beak Lake 1 sediment core (top panel), Beak Lake 2 (middle panel) and Beak Lake 3 (lower panel) showing diatom species data, including species with a relative abundance exceeding 5%.

which are predicted to have take place within West Antarctica by this model. When comparing the data to the IJ05 predictions, the best fit is again achieved with a relatively weak lower mantle viscosity, but otherwise the predictions are relatively insensitive to variations in the Earth model. We therefore adopt an optimal earth model for the IJ05 and Huybrechts models which has a lithospheric thickness of 96 km, and upper mantle viscosity of 0.5×10^{21} Pa s, and a lower mantle viscosity of 10^{22} Pa s.

The misfits highlighted in the model-data comparison (Fig. 7) cannot be rectified by further tuning the 1D earth model, suggesting that existing ice sheet reconstructions for this region must be updated in order to satisfy the new field constraints. The rate of

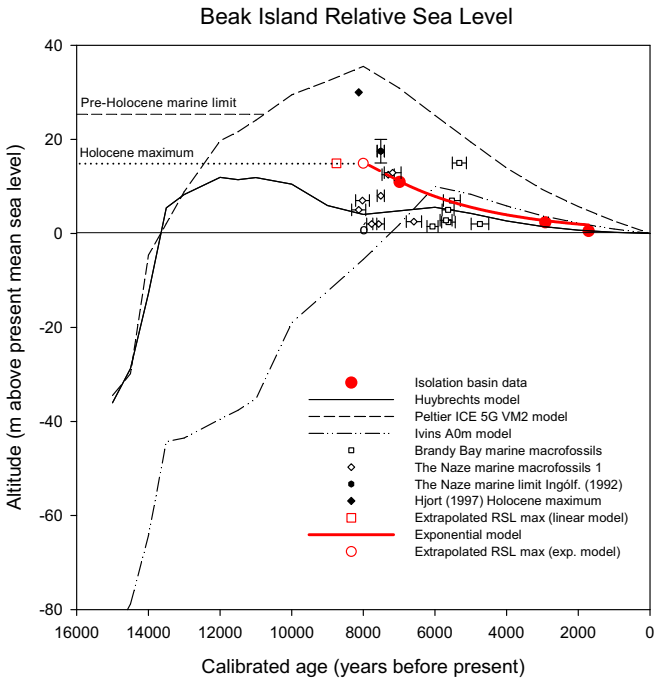

Fig. 7. Relative sea-level curve for Beak Island based on isolation basin data and surveyed marine limits compared with a suite of isostatically coupled relative sea-level models and marine macrofossils deposited on nearby James Ross Island. Isolation dates are from the freshwater end of the transition zones and errors for these dates are displayed in Table 2. The date of the Holocene marine limit on Beak Island is extrapolated both from an exponential curve fitted to the isolation basin data (open red circle) and from a linear model (open red square). The isostatically coupled relative sea-level models are the Huybrechts model (Huybrechts, 2002), the ICE-5G model (Peltier, 2004), and the Ivins A0 model (Ivins and James, 2005). Marine macrofossils were deposited on James Ross Island at Brandy Bay (Hjört et al., 1997), and The Naze (Ingólfsson et al., 1992; Hjört et al., 1997, labelled 1 and 2 respectively). Hjört et al., (1997) tentative suggestion of the marine limit on James Ross Island inferred from beach gravels with a distinct lag of beach pebbles on top is marked with a filled black circle. (For interpretation of the references to colour in this figure legend, the reader is referred to the web version of this article.)

late Holocene RSL change is most accurately reproduced by the IJ05 and Huybrechts (2002) models, during which time the dominant contribution to RSL change comes from solid earth rebound rather than a change in sea surface height. However, the rapid RSL rise prior to 6000 cal yr BP predicted by the IJ05 model does not agree with the new field data, which suggest that solid earth rebound outpaced eustatic sea-level rise for several thousand years prior to 6 ka BP. The Huybrechts (2002) model does capture this feature, suggesting that a re-analysis of the deglacial history prescribed by Ivins and James (2005) and Huybrechts (2002) should enable the model-data fit to be improved. In particular, (i) the local timing of deglaciation in the IJ05 model should be earlier, (ii) the local magnitude of LGM ice loading can be increased in both models, and (iii) a more detailed investigation of the sensitivity of the GIA model predictions to lateral variations in mantle viscosity should be carried out. The ICE-5G model requires more extensive alterations in order to fit the new RSL data.

4. Discussion

Because they reflect former ice volume changes, RSL curves are central to a number of ongoing important debates. These include determining the volume of different sectors of the Antarctic Ice Sheet at the LGM (Bentley, 1999); testing the hypothesis that Meltwater Pulse 1A was derived from Antarctica (e.g. Peltier, 2005; Bassett et al., 2007; Mackintosh et al., 2011); and determining the timing and style of deglaciation around the ice sheet margin (Conway et al., 1999). One of the most important applications of existing and new RSL curves is to constrain coupled models of ice sheet volume change and glacial isostatic adjustment. These models attempt to infer reasonable ice sheet histories by testing which histories can satisfy the constraints provided by far-field and near-field RSL datasets. Initial modelling studies have yielded promising results on former ice sheet volume (e.g. Peltier, 2004), but the limited distribution of Antarctic RSL data based on field observations means that the models are still not as well-constrained as for other continents.

The minimum radiocarbon age for deglaciation of Beak Island is c. 10,408–10,818 cal yr BP based on the onset of marine sedimentation in Beak Lake 1 (Table 2). Cosmogenic exposure ages from James Ross Island and Seymour Island suggest that ice retreated from the outer to the mid shelf close to Seymour Island between 18.3 ka and 7.3 ka, and deglaciation close to present day limits was broadly complete by c. 7.5 ka (Johnson et al., in press). The RSL history of Beak Island is consistent with this early Holocene deglaciation history and is typical of sites close to the margin of formerly expanded ice sheets, which show an early Holocene maximum, or 'high stand', followed by gradual fall to the present day. This shape occurs because the amount of glacio-isostatic rebound at the northern Antarctic Peninsula ice margin in the early Holocene was sufficiently small that eustatic sea-level rise was able to outpace it. When the northern ice sheets had melted and eustatic sea-level rise slowed, isostatic rebound outpaced the eustatic signal, leading to a slow RSL fall.

4.1. Local comparisons

The measured altitude (14.91 m) and extrapolated timing (c. 8000 cal yr BP, based on a logarithmic function) of the RSL maximum at Beak Island is similar in altitude but slightly predates the 15–20 m post-7920+/−60 ^{14}C yr BP (7512 cal yr BP) RSL maximum cited by Ingólfsson et al. (1992, p. 219) on nearby James Ross Island (Fig. 7). Furthermore, it is lower in altitude and predates the 16 m RSL maximum at c. 5885+/−65–5455+/−90 ^{14}C yr BP (5319–4744 cal yr BP) cited by Hjört et al., (1997, p. 263 and 269), also on James Ross Island. These maxima are based on radiocarbon dates of the marine bi-valve *Laternula elliptica* and *Yolida eightsii* in stratigraphic sequences at The Naze and Brandy Bay (35 km and 42 km distant respectively; marked '1' and '2' on Fig. 1). Compared with regional marine limits, the RSL maximum at Beak Island is probably contemporaneous with the well developed beach ridges up to 18 m a.s.l. at Comb Ridge on the Naze (Hjört et al., 1997), and the abrasional slope ending in a cliff at 16 m a.s.l. in Brandy Bay, suggesting a c. 1–3 m difference in RSL history. At least some of this difference may be attributable to local deglaciation variations and surveying error (Hjort measured beaches using a combination of digital altimetry citing an error of ±2 m and hand-held mirror altimetry citing an error of ±1 m). However, we have also calculated RSL predictions for these sites using a range of glacio-isostatic models, and the 2–3 m difference in Holocene marine maximum between Beak Island and James Ross Island is supported by the models, and can be demonstrated to be part of a regional trend along the Antarctic Peninsula.

We consider the 'tentative marine limit of 30 m', cited by Hjört et al., (1997, pp. 263 and 269) at 8560+/−100 ^{14}C yr BP (8131 cal yr BP; marked by a filled circle on Fig. 7), more likely to be an earlier Quaternary marine limit, and possibly congruent with the marine limit at 25.31 m on Beak Island (Table 1; Fig. 2, marine limit 2). The presence of marine shells of MIS3 age at Cape Lachmann (30 km distant) and St Martha Cove (42 km distant) at heights ranging from 0–18 m a.s.l. (Ingólfsson et al., 1992) may provide a constraining age

for this shoreline, similar to evidence for an MIS3 RSL high stand elsewhere in Antarctica (Miura et al., 1998; Hodgson et al., 2009).

Exotic boulder zones mapped on Beak Island provide further evidence of higher relative sea-levels in the past. Plutonic/sedimentary boulders deposited on low altitude raised beaches in Zones 1 and 2 (Z1 and Z2 in Fig. 3) were most likely deposited in the Holocene as icebergs rich in ice-rafted debris became 'grounded' by the wind/currents in Bay C. A similar process was observed on the modern day beach. The more substantial boulder fields across the higher altitude central part of the island (Zones Z3–7) most likely represent areas where larger icebergs became grounded when relative sea-level was significantly higher.

As Beak Island is composed of extrusive igneous rocks, the boulders found must have been transported from plutonic/sedimentary outcrops on the Antarctic Peninsula. Similar well-rounded plutonic boulders were also found on raised and present day beaches of James Ross Island, with some apparently recently 'excavated' from substantial drift deposits. Rounded granitic erratics sampled for cosmogenic exposure dating on Beak Island have a complicated and poorly constrained depositional and exposure history compared to the plateaux boulders sampled in Johnson et al. (in press) which were deposited and have remained *in-situ* as the ice sheet in the area thinned. Nevertheless, if inheritance and recycling do not present insurmountable obstacles, cosmogenic surface exposure dating of rounded granitic erratics and other exotic ice-rafted debris from the shorelines and intra-lake areas of Beak Island could provide independent constraints on the ages of Holocene and earlier marine limits, as could OSL dating of beach cobble surfaces on the shorelines (cf. Simms et al., 2011).

Our reconstructed RSL curve does not show any evidence of local Holocene glacier readvances, which would delay isostatic recovery, most likely because local glacier source areas are largely absent on Beak Island. In contrast, Holocene readvances have been inferred from the emplacement of glaciomarine deposits over glacial till at The Naze on James Ross Island between 8460+/−90 and 7920+/−60 ^{14}C yr BP (8023–7512 cal yr BP) (Ingólfsson et al., 1992, p. 213), a short-lived readvance of glaciers into Brandy Bay between 5000–4500 ^{14}C yr BP (c. 5510–5080 cal yr BP) (Hjört et al., 1997, p. 271) associated with the Bahía Bonita glacial drift (Rabassa, 1983; Björck et al., 1996) and proxy evidence of high water levels in Terrapin Lake (James Ross Island) associated with 'probable' glacial advances between 4200 ^{14}C yr BP until around 3000 ^{14}C yr BP (4645–3110 cal yr BP) (Björck et al., 1996, p. 215). As these glacial advances are local to James Ross Island, they will have only modified the local RSL history, with little or no impact on regional isostatic recovery.

4.2. Regional comparisons

The RSL maximum at Beak Island is similar in altitude and age to the 15.5 m RSL maximum on the South Shetland Islands to the west of the Antarctic Peninsula (180 km distant), which is dated between c. 8000 and 7000 cal yr BP (Watcham et al., 2011). In contrast, the Beak Island RSL maximum postdates the linear extrapolated c. 9000 yr BP maximum inferred from Marguerite Bay 630 km further south on the west side of the Antarctic Peninsula (Bentley et al., 2005), where RSL reached an altitude of 41 m a.s.l. (unpublished British Antarctic Survey data from Calmette Bay). The Calmette Bay marine limit points an enhanced isostatic depression resulting from the substantial ice stream that occupied Marguerite Bay, draining north-western catchments of the West Antarctic Ice Sheet (Bentley et al., in press). Thus, the timing of the inferred RSL maxima in the Antarctic Peninsula region ranges from c. 8000 (Beak Island) to c. 8000–7000 cal yr BP (South Shetland Islands) to c. 9000 yr BP (Marguerite Bay).

A similar range of dates for the RSL maximum is evident at sites along the East Antarctic coast where the high stand occurs at c. 9 m from c. 9260–8650 until c. 7570–7270 cal yr B P in the Larsemann and Vestfold Hills (Verleyen et al., 2005), at c. 20 m around 8440+/−140 ^{14}C yr BP (7719–8303 cal yr BP after correction for the marine reservoir effect) along the Syowa Coast (Miura et al., 1998), at 31.5 m around 8160+/−300 ^{14}C yr BP (7178–8343 cal yr BP after correction for the marine reservoir effect) in the Windmill Islands (Goodwin and Zweck, 2000), and at an estimated 32 m from 7900 ^{14}C yr BP (7406–7589 cal yr BP after correction for the marine reservoir effect) on the Ross Sea coast (Hall et al., 2004), with the different maxima reflecting variations in regional ice sheet volume and the timing of the onset of deglaciation. Although these RSL maxima were driven primarily by a decrease in the rate of eustatic sea-level rise, they are modified by the local isostatic response to ice loading and unloading. Future ice sheet reconstructions should seek to reproduce these regional variations when coupled with GIA model simulations.

The later timing of the RSL maximum in the Larsemann and Vestfold Hills suggests that this part of the East Antarctic Ice sheet began deglaciating later than other areas (for which data are available) so that isostatic recovery was unable to equal or outpace eustatic sea-level rise until around 7500 yr BP.

Improving estimates of the Antarctic contribution to global sea-level relies on an iterative process between data and models. The data provided here provide geological constraints that will be of use to modellers to improve the prediction of ice sheet volume and extent over the Antarctic Peninsula after the LGM, and its contribution to sea-level rise during the subsequent deglaciation (e.g. Huybrechts, 1990; Nakada et al., 2000; Bassett et al., 2007). The new data complement existing data to the west of the Antarctic Peninsula, thus providing a unique opportunity for future research into deglaciation differences east and west of the Antarctic Peninsula. The tight constraints on late Holocene RSL rates provided by the data in this paper will also serve as a useful comparison for future observations of RSL and solid earth rebound, which are likely to be dominated by the response to present day ice mass changes.

5. Conclusions

1) Isolation basins and geomorphological evidence of former marine limits on Beak Island provide geological constraints on Holocene RSL change for the north-eastern Antarctic Peninsula.
2) The sequential isolation of three lake basins at different altitudes during the Holocene was determined using a combination of sedimentological, microfossil and biogeochemical analyses. The timing of isolation was determined by a combination of moss macrofossil, microbial mat macrofossil, and bulk sediment radiocarbon ages.
3) RSL on Beak Island fell from a maximum of 14.91 m at c. 8000 cal yr BP at a rate of 3.91 mm per year, declining to 2.11 mm per year between 6988 and 2920 cal yr BP, 1.63 mm per year between 2920 and 1787 cal yr BP, and finally to 0.29 mm per year during the last 1787 cal yr. There is no evidence of glacial still stands or major readvances on Beak Island.
4) The Beak Island RSL curve improves the spatial coverage of RSL data in the Antarctic, and can be used to constrain glacio-isostatic adjustment models for this location. It provides well-constrained data for the glacial isostatic correction required by satellite-gravity derived measurements of contemporary ice mass loss, which are being used to assess the future contribution of the Antarctic Peninsula Ice Sheet to rising sea-levels.

Acknowledgements

This study was funded by the NERC British Antarctic Survey QUATSED project (led by D.A. Hodgson) and the Belgian Science Policy Office project HOLANT (led by W. Vyverman). E. Verleyen is a postdoctoral research fellow of the Fund for Scientific Research Flanders, Belgium. Peter Fretwell assisted with processing the GPS data. Andy Lole is thanked for his assistance in the field. The British Antarctic Survey and the captain and crew of the HMS Endurance and 815 Naval Air Squadron provided logistic support. We thank Maarten Blaauw and Christopher Bronk-Ramsey for their help with CLAM and OXCAL-related questions and Erik Ivins, Philippe Huybrechts and Richard Peltier for providing their models.

References

Agostinetti, P.N., Spada, G., Cianetti, S., 2004. Mantle viscosity inference: a comparison between simulated annealing and neighbourhood algorithm inversion methods. Geophysical Journal International 160, 890–900.

Bassett, S.E., Milne, G.A., Bentley, M.J., Huybrechts, P., 2007. Modelling Antarctic sea-level data to explore the possibility of a dominant Antarctic contribution to meltwater pulse IA. Quaternary Science Reviews 26, 2113–2127.

Battarbee, R.W., Kneen, M.J., 1982. The use of electronically counted microspheres in absolute diatom analysis. Limnology and Oceanography 27, 184–188.

Bentley, M.J., 1999. Volume of Antarctic Ice at the Last Glacial Maximum, and its impact on global sea level change. Quaternary Science Reviews 18 (14), 1569–1595.

Bentley, M.J., Hodgson, D.A., Smith, J.A., Cox, N.J., 2005. Relative sea level curves for the south Shetland islands and Marguerite Bay, Antarctic Peninsula. Quaternary Science Reviews 24, 1203–1216.

Bentley, M.J., Johnson, J.S., Hodgson, D.A., Dunai, T., Freeman, S., Ó Cofaigh, C., in press. Rapid deglaciation of Marguerite Bay, western Antarctic Peninsula in the early Holocene. Quaternary Science Reviews.

Bibby, J.S., 1966. The stratigraphy of part of north-east Graham land and the James Ross island group. British Antarctic Survey Scientific Reports 53, pp. 37.

Björck, S., Håkansson, H., Zale, R., Karlen, W., Jonsson, B.L., 1991a. A late Holocene sediment sequence from Livingston Island, South Shetland Islands, with palaeoclimatic implications. Antarctic Science 3 (1), 61–72.

Björck, S., Hjort, C., Ingólfsson, O., Skog, G., 1991b. Radiocarbon dates from the Antarctic Peninsula – problems and potential. In: Lowe, J.J. (Ed.), Radiocarbon Dating: Recent Applications and Future Potential. Quaternary Proceedings. Quaternary Research Association, Cambridge, pp. 55–65.

Björck, S., Olsson, S., Ellis-Evans, J.C., Häkansson, H., Humlum, O., de Lirio, J.M., 1996. Late Holocene palaeoclimatic records from lake sediments on James Ross island, Antarctica. Palaeogeography Palaeoclimatology Palaeoecology 121 (3–4), 195–220.

Blaauw, M., 2010. Methods and code for 'classical' age-modelling of radiocarbon sequences. Quaternary Geochronology 5, 512–518.

Bronk Ramsey, C., 2001. Development of the radiocarbon calibration program OxCal. Radiocarbon 43 (2A), 355–363.

Clapperton, C., 1969. The volcanic eruption at Deception island, December 1967. British Antarctic Survey Bulletin 22, 83–90.

Clark, P.U., Mitrovica, J.X., Milne, G.A., Tamisiea, M.E., 2002. Sea-level fingerprinting as a direct test for the source of global meltwater pulse IA. Science 295 (5564), 2438–2441.

Conway, H., Hall, B.L., Denton, G.H., Gades, A.M., Waddington, E.M., 1999. Past and future grounding line retreat of the West Antarctic Ice Sheet. Science 286, 280–283.

Cook, A.J., Fox, A.J., Vaughan, D.G., Ferrigno, J.G., 2005. Retreating glacier fronts on the Antarctic Peninsula over the past half-century. Science 308, 541–544.

Dean, W.E., 1974. Determination of carbonate and organic matter in calcareous sediments and sedimentary rocks by loss on ignition, comparison with other models. Journal of Sedimentary Petrology 44, 242–248.

Fleming, K., Johnston, P., Zwartz, D., Yokoyama, Y., Lambeck, K., Chappell, J., 1998. Refining the eustatic sea-level curve since the Last Glacial Maximum using far and intermediate-field sites. Earth and Planetary Science Letters 163, 327–342.

Fretwell, P.T., Hodgson, D.A., Watcham, E., Bentley, M.J., Roberts, S.J., 2010. Holocene isostatic uplift of the South Shetland Islands, Antarctic Peninsula, modelled from raised beaches. Quaternary Science Reviews 29 (15–16), 1880–1893.

Goodwin, I.D., Zweck, C., 2000. Glacio-isostasy and glacial ice load at Law Dome, Wilkes land, east Antarctica. Quaternary Research 53 (3), 285–293.

Grimm, E.C., 1987. CONISS, a FORTRAN-77 program for stratigraphically constrained cluster analysis by the method of incremental sum of squares. Computers and Geosciences 13, 13–35.

Hall, B.L., Baroni, C., Denton, G.H., 2004. Holocene relative sea-level history of the southern Victoria Land coast, Antarctica. Global and Planetary Change 42 (1–4), 241–263.

Hall, B.L., 2010. Holocene relative sea-level changes and ice fluctuations in the South Shetland Islands. Global and Planetary Change 74, 15–26.

Hjört, C., Ingólfsson, O., Möller, P., Lirio, J.M., 1997. Holocene glacial history and sea-level changes on James Ross Island, Antarctic Peninsula. Journal of Quaternary Science 12 (4), 259–271.

Hodgson, D.A., Dyson, C.L., Jones, V.J., Smellie, J.L., 1998. Tephra analysis of sediments from Midge Lake (South Shetland Islands) and Sombre Lake (South Orkney Islands), Antarctica. Antarctic Science 10 (1), 13–20.

Hodgson, D.A., Bentley, M.J., Roberts, S.J., Smith, J.A., Sugden, D.E., Domack, E.W., 2006. Examining Holocene stability of Antarctic Peninsula ice shelves. Eos Transactions, American Geophysical Union 87, 305–312.

Hodgson, D.A., Verleyen, E., Vyverman, W., Sabbe, K., Leng, M.J., Pickering, M., Keely, B.J., 2009. A geological constraint on relative sea level in Marine Isotope Stage 3 in the Larsemann Hills, Lambert Glacier region, east Antarctica (31,366–33,228 cal yr BP). Quaternary Science Reviews 28, 2689–2696.

Holland, P.R., Jenkins, A., Holland, D.M., 2008. The response of ice-shelf basal melting to variation in ocean temperature. Journal of Climate 15, 2558–2572.

Houghton, J.T., Ding, Y., Griggs, D.J., Noguer, M., van der Linden, P.J., Dai, X., Maskell, K., Johnson, C.A., 2001. Climate Change 2001: The Scientific Basis. Contribution of Working Group I to the Third Assessment Report of the Intergovernmental Panel on Climate Change. Cambridge University Press, 944 pp.

Hua, Q., Barbetti, M., 2004. Review of tropospheric bomb C-14 data for carbon cycle modeling and age calibration purposes. Radiocarbon 46, 1273–1298.

Huybrechts, P., 1990. A 3-D model for the Antarctic ice sheet: a sensitivity study on the glacial-interglacial contrast. Climate Dynamics 5, 79–92.

Huybrechts, P., 1992. The Antarctic ice sheet and environmental change: a three-dimensional modeling study. Berichte Für Polarforschung 99, 1–241.

Huybrechts, P., 2002. Sea-level changes at the LGM from ice-dynamic reconstructions of the Greenland and Antarctic ice sheets during the glacial cycles. Quaternary Science Reviews 21 (1–3), 203–231.

Ingólfsson, Ó, Hjort, C., Bjorck, S., Smith, R.I.L., 1992. Late Pleistocene and Holocene glacial history of James-Ross-Island, Antarctic Peninsula. Boreas 21 (3), 209–222.

Ivins, E.R., James, T.S., 2005. Antarctic glacial isostatic adjustment: a new assessment. Antarctic Science 17 (04), 541–553.

Jansen, E.J., Overpeck, K.R., Briffa, J.-C., Duplessy, F., Joos, V., Masson-Delmotte, D., Olago, B., Otto-Bliesner, W.R., Peltier, S., Rahmstorf, R., Ramesh, D., Raynaud, D., Rind, O., Solomina, R., Villalba, R., Zhang, D., 2007. Palaeoclimate. In: Solomon, S.D., et al. (Eds.), Climate Change 2007: The Physical Science Basis. Contribution of Working Group I to the Fourth Assessment Report of the Intergovernmental Panel on Climate Change. Cambridge University Press, Cambridge, United Kingdom and New York, NY, USA, pp. 433–497.

Johnson, J.S., Bentley, M.J., Roberts, S.J., Binnie, S.A. and Freeman, S. Holocene deglacial history of the north east Antarctic Peninsula. Quaternary Science Reviews, in press.

Kopp, R.E., Simons, F.J., Mitrovica, J.X., Maloof, A.C., Oppenheimer, M., 2009. Probabilistic assessment of sea level during the Last Interglacial stage. Nature 462, 863–867.

Lambeck, K., Smither, C., Johnston, P., 1998. Sea-level change. Geophysical Journal International 134, 102–144.

Lee, Y.I., Limb, H.S., Yoon, H.I., Tatur, A., 2007. Characteristics of tephra in Holocene lake sediments on King George Island, West Antarctica: implications for deglaciation and paleoenvironment. Quaternary Science Reviews 26, 3167–3178.

Livingstone, D.A., 1955. A lightweight piston sampler for lake deposits. Ecology 36, 137–139.

Mackintosh, A., Golledge, N., Domack, E., Dunbar, R., Leventer, A., White, D., Pollard, D., DeConto, R., Fink, D., Zwartz, D., Gore, D., Lavoie, C., 2011. Retreat of the East Antarctic ice sheet during the last glacial termination. Nature Geoscience doi: 10.1038/NGEO1061.

McCormac, F., Hogg, A., Blackwell, P., Buck, C., Higham, T., Reimer, P., 2004. Shcal04 Southern Hemisphere calibration 0–11.0 cal kyr BP. Radiocarbon 46, 1087–1092.

Meyers, P.A., Teranes, J.L., 2001. Sediment organic matter. In: Last, W.M., Smol, J.P. (Eds.), Tracking Environmental Change Using Lake Sediments. Physical and Geochemical Methods, vol. 2. Kluwer, Dordrecht, The Netherlands, pp. 239–269.

Miura, H., Maemoku, H., Igarishi, A., Moriwaki, K., 1998. Late Quaternary Raised Beach Deposits and Radiocarbon Dates of Marine Fossils Around Lützow-Holm Bay. Special Map Series of National Institute of Polar Research, Tokyo. vol. 6.

Nakada, M., Lambeck, K., 1988. The melting history of the late Pleistocene Antarctic Ice-Sheet. Nature 333, 36–40.

Nakada, M., Kimura, R., Okuno, J., Moriwaki, K., Miura, H., Maemoku, H., 2000. Late Pleistocene and Holocene melting history of the Antarctic ice sheet derived from sea-level variations. Marine Geology 167 (1–2), 85–103.

Ochyra, R., 2008. Mosses of the Prince Edward Islands. In: Chown, R.S., Froneman, P.W. (Eds.), Prince Edward Islands. Sun Press, Stellenbosch, South Africa, pp. 383–389.

Peltier, W.R., 1998. Postglacial variations in the level of the sea: implications for climate dynamics and solid-Earth geophysics. Reviews of Geophysics 36 (4), 603–689.

Peltier, W.R., 2004. Global glacial isostasy and the surface of the ice-age earth: the ICE-5G(VM2) model and GRACE. Annual Review of Earth and Planetary Sciences 32, 111–149.

Peltier, W.R., 2005. On the hemispheric origins of meltwater pulse 1a. Quaternary Science Reviews 24 (14–15), 1655–1671.

Pfeffer, W.T., Harper, J.T., O'Neel, S., 2008. Kinematic constraints on glacier contributions to 21st-century sea-level rise. Science 321 (5894), 1340–1343.

Philippon, G., Ramstein, G., Charbit, S., Kageyama, M., Ritz, C., Dumas, C., 2006. Evolution of the Antarctic ice sheet throughout the last deglaciation: a study with a new coupled climate-north and south hemisphere ice sheet model. Earth and Planetary Science Letters 248 (3–4), 750–758.

Pritchard, H.D., Vaughan, D.G., 2007. Widespread acceleration of tidewater glaciers on the Antarctic Peninsula. Journal of Geophysical Research 112 (F3), F03S29.

Rabassa, J., 1983. Stratigraphy of the glacigenic deposits in northern James Ross Island, Antarctic Peninsula. In: Evenson, E., Schlüchter, C., Rabassa, J. (Eds.), Tills and Related Deposits. A.A. Balkema Publishers, Rotterdam, pp. 329–340.

Rahmstorf, S., 2007. A semi-empirical approach to projecting future sea-level rise. Science 315 (5810), 368–370.

Reimer, P.J., Baillie, M.G.L., Bard, E., Bayliss, A., Beck, J.W., Bertrand, C.J.H., Blackwell, P.G., Buck, C.E., Burr, G.S., Cutler, K.B., Damon, P.E., Edwards, R.L., Fairbanks, R.G., Friedrich, M., Guilderson, T.P., Hogg, A.G., Hughen, K.A., Kromer, B., McCormac, G., Manning, S., Ramsey, C.B., Reimer, R.W., Remmele, S., Southon, J.R., Stuiver, M., Talamo, S., Taylor, F.W., Van Der Plicht, J., Weyhenmeyer, C.E., 2004a. Intcal04 Terrestrial radiocarbon age calibration, 0–26 cal kyr BP. Radiocarbon 46, 1029–1058.

Reimer, P.J., Brown, T.A., Reimer, R.W., 2004b. Discussion: reporting and calibration of post-bomb ^{14}C data. Radiocarbon 46, 1299–1304.

Reimer, P.J., Baillie, M.G.L., Bard, E., Bayliss, A., Beck, J.W., Blackwell, P.G., Bronk Ramsey, C., Buck, C.E., Burr, G.S., Edwards, R.L., Friedrich, M., Grootes, P.M., Guilderson, T.P., Hajdas, I., Heaton, T.J., Hogg, A.G., Hughen, K.A., Kaiser, K.F., Kromer, B., McCormac, F.G., Manning, S.W., Reimer, R.W., Richards, D.A., Southon, J.R., Talamo, S., Turney, C.S.M., van der Plicht, J., Weyhenmeyer, C.E., 2009. IntCal09 and Marine09 radiocarbon age calibration curves, 0-50,000 years cal BP. Radiocarbon 51, 1111–1150.

Reimer, P.J., Reimer, R., 2011. CALIBomb Radiocarbon Calibration Program. http://calib.qub.ac.uk/CALIBomb/.

Renberg, I., 1990. A procedure for preparing large sets of diatom slides from sediment cores. Journal of Paleolimnology 4, 87–90.

Rignot, E., Bamber, J.L., van den Broeke, M.R., Davis, C., Li, Y., Jan van de Berg, W., van Meijgaard, E., 2008. Recent Antarctic ice mass loss from radar interferometry and regional climate modelling. Nature Geoscience 1, 106–110. doi:10.1038/ngeo102.

Roberts, S.J., Hodgson, D.A., Bentley, M.J., Sanderson, D.C.W., Milne, G.A., Smith, J.A., Verleyen, E., Balbo, A., 2009. Holocene relative sea-level change and deglaciation on Alexander Island, Antarctic Peninsula from elevated lake deltas. Geomorphology 112 (1–2), 122–134.

Sime, L.C., Wolff, E.W., Oliver, K.I.C., Tindall, J.C., 2009. Evidence for warmer Interglacials in East Antarctic ice cores. Nature 462, 342–345.

Simms, A.R., DeWitt, R., Kouremenos, P., Drewrya, A.M., 2011. A new approach to reconstructing sea levels in Antarctica using optically stimulated luminescence of cobble surfaces. Quaternary Geochronology 6, 50–60.

Solomon, S., Qin, D., Manning, M., Chen, Z., Marquis, M., Averyt, K.B., Tignor, M., Miller, H.L., 2007. Contribution of Working Group I to the Fourth Assessment Report of the Intergovernmental Panel on Climate Change. Cambridge University Press, Cambridge, United Kingdom and New York, NY, USA, 996 pp.

Steig, E.J., Schneider, D.P., Rutherford, S.D., Mann, M.E., Comiso, J.C., Shindell, D.T., 2009. Warming of the Antarctic ice-sheet surface since the 1957 International Geophysical Year. Nature 457, 459–462.

Sterken, M., Roberts, S.J., Hodgson, D.A., Vyverman, W., Balbo, A., Sabbe, K., Moreton, S.G. and Verleyen, E. Holocene glacial and climate history of Prince Gustav Channel, northeastern Antarctic Peninsula. Quaternary Science Reviews, in press, doi:10.1016/j.quascirev.2011.10.017.

Sugden, D.E., John, B., 1973. The Ages of Glacier Fluctuations in the South Shetland Islands, Antarctica. In: Palaeoecology of Africa, the Surrounding Islands and Antarctica. Balkema, Cape Town, pp. 141–159.

Vaughan, D.G., Doake, C.S.M., 1996. Recent atmospheric warming and retreat of ice shelves on the Antarctic Peninsula. Nature 379, 328–331.

Verleyen, E., Hodgson, D.A., Milne, G.A., Sabbe, K., Vyverman, W., 2005. Relative sea level history from the Lambert Glacier region (East Antarctica) and its relation to deglaciation and Holocene glacier re-advance. Quaternary Research 63, 45–52.

Watcham, E.P., Bentley, M.J., Hodgson, D.A., Roberts, S.J., Fretwell, P.T., Lloyd, J.M., Larter, R.D., Whitehouse, P.L., Leng, M.J., Monien, P., Moreton, S.G., 2011. A new relative sea level curve for the South Shetland Islands, Antarctica. Quaternary Science Reviews 30, 3152–3170.

Willmott, V., Domack, E.W., Canals, M., Brachfeld, S., 2006. A high resolution relative paleointensity record from the Gerlache-Boyd paleo-ice stream region, northern Antarctic Peninsula. Quaternary Research 66, 1–11.

Zwartz, D., Bird, M., Stone, J., Lambeck, K., 1998. Holocene sea-level change and ice-sheet history in the Vestfold Hills, East Antarctica. Earth and Planetary Science Letters 155 (1–2), 131–145.